Numerical Prediction of Convectively Driven Mesoscale Pressure Systems. Part I: Convective Parameterization

J. M. FRITSCH AND C. F. CHAPPELL

Atmospheric Physics and Chemistry Laboratory, NOAA, Boulder, CO 80303

(Manuscript received 2 February 1979, in final form 10 April 1980)

ABSTRACT

A parameterization formulation for incorporating the effects of midlatitude deep convection into mesoscale numerical models is presented. The formulation is based on the hypothesis that the buoyant energy available to a parcel, in combination with a prescribed period of time for the convection to remove that energy, can be used to regulate the amount of convection in a mesoscale numerical model grid element.

Individual clouds are represented as entraining moist updraft and downdraft plumes. The fraction of updraft condensate evaporated in moist downdrafts is determined from an empirical relationship between the vertical shear of the horizontal wind and precipitation efficiency. Vertical transports of horizontal momentum and warming by compensating subsidence are included in the parameterization. Since updraft and downdraft areas are sometimes a substantial fraction of mesoscale model grid-element areas, grid-point temperatures (adjusted for convection) are an area-weighted mean of updraft, downdraft and environmental temperatures.

1. Introduction

The theory of cumulus parameterization can be traced back to the development of numerical prediction models which included moist adiabatic processes. Smagorinsky (1956) introduced the first cumulus parameterization when he adjusted the vertical derivative of an "effective static stability" which included the heat liberated during condensation. This adjustment, which in concept dates back to the early work of Rossby (1932), was the forerunner of several "convective adjustment" techniques that were used in later models (see, e.g., Mintz, 1965; Manabe *et al.*, 1965; Oliger *et al.*, 1970; Gadd and Newson, 1969).

With the recognition that tropical storms are driven in part by deep cumulonimbus convection, it became important to understand how deep convection interacts with its large-scale environment, and to introduce these effects into tropical storm models. From this impetus came new approaches to parameterization which are generally classified as penetrative convective techniques. These techniques attempt to relate a large-scale mass, moisture or energy budget to the integrated convective activity, while using some form of "cloud model" to vertically redistribute mass, moisture and energy (e.g., Kuo, 1965, 1974; Ooyama, 1971; Ogura and Cho, 1973; Fraedrich, 1974; Anthes, 1977).

Ooyama (1963) and Charney and Eliassen (1964) recognized the importance of surface friction in producing low-level convergence and thereby supplying latent heat energy to larger scale systems. Other investigators who linked low-level frictional convergence on the large scale to the cumulus scale include Yamasaki (1968), Rosenthal (1970), Ooyama (1969) and Chang and Piwowar (1974). Studies by Ceselski (1974), however, indicate that frictional pumping is neither a necessary nor a sufficient cause for the occurrence of cumulus convection.

Another large-scale control was introduced by Arakawa and Schubert (1974). They assumed that the rate of stabilization by an ensemble of cumulus clouds balances the rate at which the large scale makes buoyant energy available for convection. Johnson (1976) modified the Arakawa-Schubert approach by incorporating moist downdrafts to offset some of the low-level subsidence warming and drying.

Finally, a unique approach to convective parameterization was introduced by Kreitzberg and Perkey in 1976. Unlike previous techniques which assume that the rate of convective mass transfer is regulated by *large-scale rates* (e.g., large-scale mass or moisture convergence), Kreitzberg and Perkey require enough convection (updraft area) so that the vertical pressure difference in the layer from cloud top to cloud base becomes the same in the environment as in the cloud column itself. Thus, the amount of convective mass transfer is free to vary according to the *local* conditions.

The present investigation is concerned with the parameterization of midlatitude organized convection into mesoscale ($\Delta x \leq 20$ km) numerical models.

A parameterization procedure and the required cloud model are presented in the next two sections.

2. Convective parameterization technique

Following Anthes (1977), the area-averaged time rate of change of mean temperature may be written as

$$\frac{\partial \bar{T}}{\partial t} + \nabla\cdot\bar{\mathbf{V}}\bar{T} + \frac{\partial \bar{\omega}\bar{T}}{\partial p} - \frac{\bar{\omega}R\bar{T}}{c_p p} = \frac{L}{c_p}\overline{C^*} - \frac{\partial \overline{\omega' T'}}{\partial p} + \frac{R\overline{\omega' T'}}{c_p p}, \quad (1)$$

where C^* is the local condensation or evaporation rate, and the overbar and prime indicate the mean and eddy components, respectively (see Appendix for list of symbols). The terms on the right-hand side of (1) are the latent heat release in the clouds and the eddy flux of sensible heat. These terms *together* define the mean temperature change produced by convection, i.e.,

$$\left.\frac{\partial \bar{T}}{\partial t}\right|_{\text{conv}} = \frac{L}{c_p}\overline{C^*} - \frac{\partial \overline{\omega' T'}}{\partial p} + \frac{R\overline{\omega' T'}}{c_p p}. \quad (2)$$

Assuming that changes produced by convection can be spread uniformly over the time period convection is active in a numerical model grid element, the convectively produced temperature change can also be expressed as

$$\left.\frac{\partial \bar{T}}{\partial t}\right|_{\text{conv}} = \frac{\hat{T} - T_0}{\tau_c}, \quad (3)$$

where T_0 is the grid element temperature before convection, $\hat{T}$ the grid element temperature after convection, and τ_c the characteristic time period that convection is active in the grid element. Thus, very simply, the convective parameterization problem is to determine $\hat{T}$ and τ_c.

Formulation of the convective parameterization follows the same general approach as other techniques. A quantity in the numerical model is selected to control the amount of convection, and a cloud model is used to estimate the vertical structure of the convective mass flux which satisfies the control. Compensating environmental vertical motions follow from mass continuity so that the vertical structure of environmental temperature changes is also specified by the cloud model.

Specification of the amount of convective activity originates with the concept of potential buoyant energy (PBE) and available buoyant energy (ABE). Consider the following: The vertical component of the equation of motion for an air parcel of unit mass in an updraft, ignoring pressure perturbations due to the updraft and frictional effects, is

$$\frac{dw}{dt} = g\left(\frac{T_U - T}{T}\right) = g\beta, \quad (4)$$

where T_U denotes the updraft temperature and T is the environmental (or grid-point) temperature. In an atmosphere containing a deep conditionally unstable layer and high relative humidity at low levels (as in Fig. 1) an air parcel rising from near the surface without mixing will achieve saturation at its lifting condensating level (LCL). Typically, $\beta < 0$ at the LCL but continued rise of the parcel in the conditionally unstable environment results in an increase of β. The parcel's level of free convection (LFC) is reached at the point where β increases past zero; the LFC is the base of the layer where $\beta > 0$. If the parcel is still rising when its LFC is reached, it will continue to rise, eventually reaching its equilibrium temperature level (ETL), where β decreases to zero. The increase in kinetic energy of the parcel, associated with its vertical acceleration in rising between its LFC and its ETL, is given by

$$\tfrac{1}{2}w^2\big|_{\text{ETL}} - \tfrac{1}{2}w^2\big|_{\text{LFC}} = \int_{\text{LFC}}^{\text{ETL}} g\beta dz. \quad (5)$$

This is defined as buoyant energy, i.e., the kinetic energy derived from buoyancy. The buoyant energy is thus proportional to the positive area in Fig. 1. Potential buoyant energy (PBE) is the buoyant energy (per unit mass) which would accrue to a parcel in rising between its LFC and ETL, assuming the parcel were able to reach its LFC. The PBE is identical to the buoyant energy for the sounding and thermodynamic trajectory of the parcel shown in Fig. 1. PBE for a parcel is zero if there exists no LFC for that parcel.

Often a parcel must overcome an appreciable depth of negative buoyancy if it is to rise to its LFC. This is shown as the negative area in Fig. 1. This negative buoyancy may be reduced or eliminated by surface heating, differential horizontal temperature or moisture advection, or lifting the conditionally unstable environment if this environment is also convectively unstable. The PBE is said to be "available" (PBE = ABE) if the negative buoyancy is eliminated or overcome.

Following Kreitzberg and Perkey (1976) it is not assumed that the amount of convection is determined solely by the instantaneous values of the explicitly forecast dependent variables. On the contrary, only after the PBE for at least some air parcels within a grid column becomes available does convection begin. (The procedure used to determine this is detailed later.) This convective activity is sufficient to remove the ABE in a *specified* period of time τ_c. The basis for this assumption follows from Fritsch *et al.* (1976) who observed that the large scale typically took many hours to generate potential buoyant energy, but once this energy became available, on the mesoscale the convection removed the energy in a small fraction of the time it took to generate it.

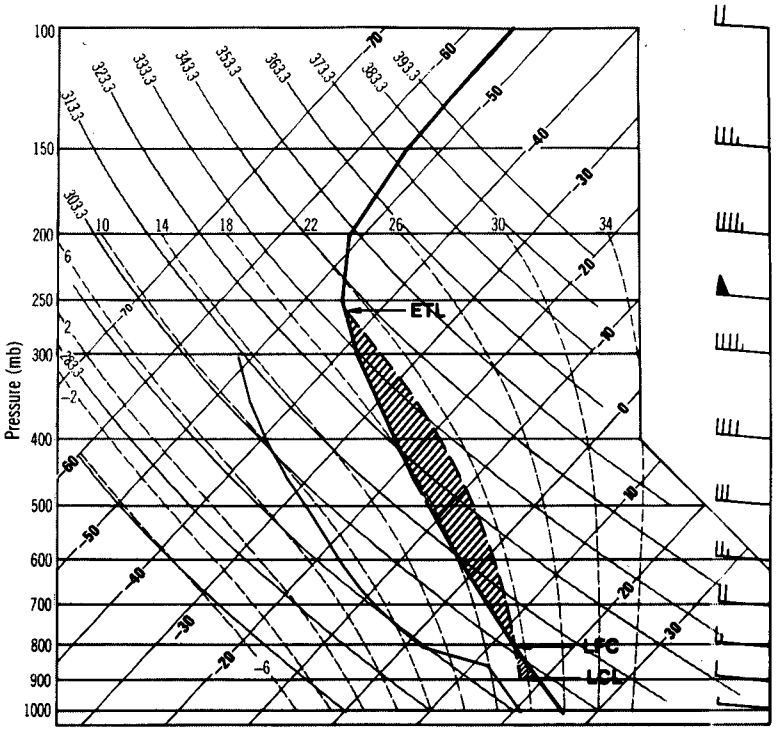

FIG. 1. Thermodynamic diagram (skew $T-\log p$) of conditionally unstable sounding. Heavy and thin solid lines indicate environmental temperature and dewpoint, respectively. The heavy dashed line is a moist adiabat for a lifted parcel with mean thermodynamic characteristics of the lowest 100 mb layer. Shaded area to the left of the environmental temperature line defines the negatively buoyant region between the lifting condensation level (LCL) and the level of free convection (LFC). Shaded area to the right of the environmental temperature line defines the positive buoyant area between the LFC and the equilibrium temperature level (ETL).

The condition of complete removal of ABE by convection after time τ_c is

$$\hat{\text{ABE}} = \int_{\hat{\text{LFC}}}^{\hat{\text{ETL}}} g\left[\frac{\hat{T}_U(z) - \hat{T}(z)}{\hat{T}(z)}\right]dz = 0, \qquad (6)$$

where the caret indicates the value of a parameter after adjustment for convection. In particular, $\hat{T}_U(z)$ is the vertical distribution of temperature in the updraft that results from lifting the convectively modified air, $\hat{T}(z)$. Since the areas of updrafts and downdrafts may be a substantial fraction of a mesoscale model grid element area, grid-point temperatures are an area-weighted mean of updraft, downdraft and environmental temperatures. Thus, the grid-point temperature adjusted for convection, $\hat{T}(z)$, is defined by

$$\hat{T}(z) = A^{-1}[T_E(z)A_E(z) + T_U(z)A_U(z) + T_D(z)A_D(z)], \qquad (7)$$

where $A = A_E + A_U + A_D$, and the subscripts E, U and D identify environment, updraft and downdraft, respectively.

Because numerical models with meso β-scale resolution require rather small grid elements (typically $\leq$20 km), it is assumed that all convective clouds in an element are alike. It is further assumed that the characteristics of the first clouds to develop in a grid element will remain relatively unchanged during the time period required to transit the grid element, unless this time is longer than 1 h. The time for clouds to move through a grid element is estimated by dividing the grid length by the mean environmental wind speed over the cloud depth. If this time period (τ_c) is greater than 1 h or if it takes longer than an hour to remove all the ABE, the initial rate of grid-scale stabilization by the convection is still applied for only 1 h. After this hour, cloud characteristics are determined again for the adjusted environment. A lower time limit for maintaining similar cloud characteristics is the lifetime of a single cell, ~30 min.

With the assumption that all convective clouds in the mesoscale grid element are alike, there is a specific area (at cloud base) of updraft and corresponding areas of downdraft and environment that will produce a vertical distribution of $\hat{T}$ that satisfies (6)

in the time period τ_c. To arrive at the proper set of areas, an iterative procedure is necessary. A first guess of the updraft area is taken to be 1% of the grid element area. For an initial unit of updraft air, the corresponding amount of downdraft air is calculated using the cloud model (described in the next section). The temperature change in the environment produced by this single updraft-downdraft "cloud" unit is obtained from the time integral (over the period τ_c) of

$$\frac{\partial T_E(z)}{\partial t} = -w_E(z)[\Gamma - \gamma(z)] - \frac{L}{c_p} w_E(z) \frac{\partial r_E(z)}{\partial z}, \quad (8)$$

where the compensating environmental vertical motion w_E is assumed to occur hydrostatically, and r_E is the environmental mixing ratio. The second term on the right hand side of (8) is the environmental cooling associated with the evaporation of condensate in the anvil.

Compensating environmental vertical motion is obtained by invoking mass continuity in the following manner. Within a grid element, the total mass transport may be defined as

$$M(z) = \rho(z)\, w(z)\, A = M_E(z) + M_U(z) + M_D(z). \quad (9)$$

Eq. (9) states that the vertical mass transport is the sum of the environmental vertical transports and the convective updrafts and downdrafts. The left-hand side of (9) is provided by the mesoscale numerical model, and M_U and M_D are determined by the cloud model. Thus

$$w_E(z) = \frac{M(z) - M_U(z) - M_D(z)}{\rho_E(z) A_E(z)}. \quad (10)$$

Normally the first guess at the updraft area (A_U') will not remove all the ABE but will only produce a reduction, ΔABE. A new estimate for the number (N) of updraft-downdraft "cloud" units which will remove all the ABE is obtained from

$$N^{(m)} = \frac{\text{ABE}}{\Delta\text{ABE}^{(m-1)}} N^{(m-1)}, \quad (11)$$

where m is the number of the iteration. Eqs. (6), (7), (8), (10) and (11) are iterated until

$$\text{ABE} - \Delta\text{ABE} = 0 \pm 0.05\text{ABE}, \quad (12)$$

which is defined as an acceptable level of convergence. Usually only four or five iterations are necessary until (12) is satisfied. The total updraft cloud area is then NA_U'.

Finally, the equations governing changes in momentum and moisture follow the same mathematical development as the mass conservation. New values of moisture and momentum, adjusted for the effects of convection, are given by

$$\hat{r}(z) = A^{-1}[r_E(z)A_E(z) + r_U(z)A_U(z) + r_D(z)A_D(z)], \quad (13)$$

$$\hat{u}(z) = A^{-1}[u_E(z)A_E(z) + u_U(z)A_U(z) + u_D(z)A_D(z)], \quad (14)$$

$$\hat{v}(z) = A^{-1}[v_E(z)A_E(z) + v_U(z)A_U(z) + v_D(z)A_D(z)], \quad (15)$$

where density effects have been omitted.

The assumptions of bulk transport and mixing of horizontal momentum are implicit within these formulations. It is assumed that no significant change in horizontal momentum occurs during the brief period of time a parcel spends in the active updrafts and downdrafts. Major alterations to parcel momentum are only permitted to occur after a parcel reaches the anvil or boundary layers. As the parcel momentum is gradually incorporated into the mesoscale governing system, environmental pressure forces are then free to act on the new momentum fields.

3. Cumulus cloud model

The cumulus parameterization procedure described in the last section depends on certain cumulus cloud properties that interact with the environment. Thus, the ability of the parameterization technique to realistically simulate the genesis and evolution of midlatitude organized convective systems depends on the characteristics of a cloud model. The model used in this study differs somewhat from conventional cloud models. This is necessary for several reasons: 1) the model cloud must be constructed a large number of times; 2) it is not economically feasible nor possible with available computer power to include sophisticated microphysics in the model; and 3) it is questionable whether current one-dimensional cloud models are applicable for the type of convection parameterized in this study. Midlatitude organized convection frequently forms into lines where large and complex cumulonimbi interact with one another and with their environment. The environment exhibits strong vertical shear in both speed and direction, and there are large horizontal and vertical moisture gradients. Most importantly, however, the structure of the circulations which develop within the cumulonimbi themselves is decidedly asymmetric. That is, the juxtaposition and tilt of the updraft and downdraft are such that the up and down circulations are non-interfering. Thus, it is not possible for a simple one-dimensional model to simulate satisfactorily these complex convective processes.

Despite the complex nature of midlatitude convective cloud systems in vertical shear, observa-

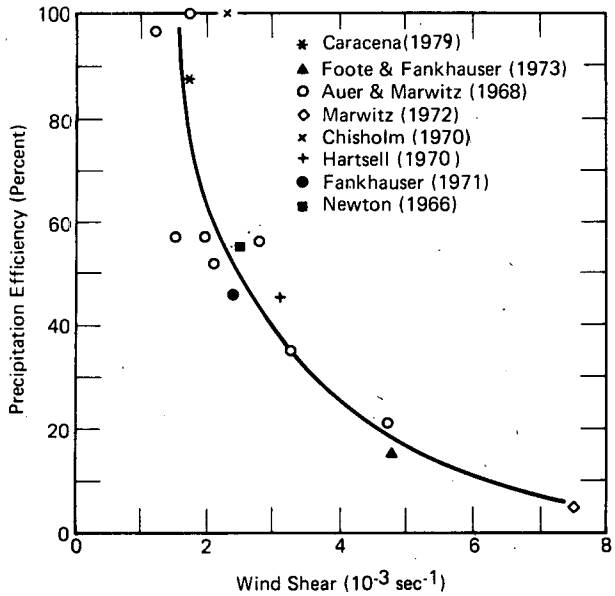

FIG. 2. Precipitation efficiency (ratio of rainout to water vapor inflow) as a function of vertical shear of the horizontal wind in the layer from cloud base to cloud top [adapted from Marwitz (1972) and Foote and Fankhauser (1973)].

tions show that simple parcel theory gives relatively good estimates of cloud-top height. This suggests a region of nearly undiluted ascent through a protected core embedded in the overall updraft area. Similarly, the study by Foster (1958) indicates that downdraft characteristics, and the level at which the main downdraft begins, can also be described satisfactorily by a parcel approach. Byers (1951) observed and computed that cumulus clouds which develop into thunderstorms entrain environmental air at a rate of ~100% per 500 mb of ascent. As a check on the impact of such entrainment rates on cloud top, the cloud model (described below) was run on several hundred soundings using a "bulk" entrainment rate of 100%, that is, all clouds doubled their mass from cloud base to cloud top. Results of the cloud model runs showed that in some instances cloud growth was damped enough that the cloud never penetrated low-level stable layers. For the most part, however, doubling the cloud mass gave cloud tops which differed from the undilute parcel ascent by only 1 km or less. Thus, a model which determines cloud-top and down-draft characteristics using an entraining parcel might be acceptable if the mass and moisture budgets could be estimated in some other manner.

Fig. 2 shows the precipitation efficiency as a function of vertical wind shear for deep convective clouds similar to the type parameterized here. This efficiency, in a crude way, is the integrated result of complex, three-dimensional interactions occurring on scales ranging from the molecular to the synoptic. By combining this cloud efficiency with entraining updraft and downdraft parcels, a simple cloud model can be constructed which includes some of the three-dimensional effects of various scale interactions, and still permits the direct determination of cloud depth and compensating environmental vertical motions.

Fig. 3 outlines the cloud model and how it interacts with the convective parameterization. The following sections define the cloud model and the information it provides to the larger scale.

a. Updraft characteristics

Beginning with the lowest 100 mb layer, a parcel with a mean layer temperature $\tilde{T}(k)$ and mixing ratio $\tilde{r}(k)$ is lifted to compute the condensation level (LCL). The parcel is checked for buoyancy using

$$T_U^s - T + \Delta T \begin{cases} >0, & \text{buoyant} \\ \leq 0, & \text{stable,} \end{cases} \tag{16}$$

where T_U^s is the temperature of the saturated updraft and T is the grid element temperature. The temperature increment ΔT is defined by

$$\Delta T = c_1 w_G^{1/3}, \tag{17}$$

where c_1 is a unit number with dimensions °C $s^{1/3}$ $cm^{-1/3}$, and w_G the mesoscale model vertical motion (cm s^{-1}) at the LCL. The temperature increment ΔT crudely simulates local perturbation forcing as a function of grid-scale motion in the layer being lifted. For example, if mesoscale lifting is 1.0 cm s^{-1}, the thermal perturbation is 1.0°C; for 10 cm s^{-1}, it is 2.15°C. In support of this type of approach, Chen and Orville (1980) have recently shown that thermals are stronger and larger when low-level convergence is present. If the parcel is stable, the 100 mb layer, 50 mb higher than the previous layer, is mixed, lifted and checked for buoyancy. This procedure is repeated up to the 600–700 mb layer where if the parcel is still stable, no convection is permitted to occur. If, however, the parcel is buoyant, the equivalent potential temperature θ^e is computed for the LCL and the parcel is lifted and mixed through 50 mb increments according to

$$\theta_U^e(k+1) = [\theta_U^e(k) M_U(k) + \Delta M_U(k) \tilde{\theta}_E^e(k)] \times [M_U(k) + \Delta M_U(k)]^{-1}, \tag{18}$$

where

$$\Delta M_U(k) = M_U(k+1) - M_U(k), \tag{19}$$

$$M_U(k) = [1 + K_U(k)] M_U(\text{LCL}), \tag{20}$$

$$\tilde{\theta}_E^e(k) = \tfrac{1}{2}[\theta_E^e(k+1) + \theta_E^e(k)], \tag{21}$$

and K_U is defined below. Eq. (18) defines the equivalent potential temperature of a parcel (with mass flux M_U) ascending moist adiabatically from

level k to $k + 1$, while entraining mass at the rate ΔM_U. The entraining mass is distributed linearly (with height) over the cloud depth so that the fractional entrainment for a layer is given by

$$\Delta K_U(k) = B_U[z(k+1) - z(k)][z_{CT} - z_{LCL}]^{-1} \quad (22)$$

and the total fraction of entrainment up to any level k is

$$K_U(k) = \sum_{q \text{ at LCL}}^{q=k} \Delta K_U(q). \quad (23)$$

The bulk mixing coefficient B_U is set equal to 1.0 which means the parcel increases its mass by 100% from cloud base to cloud top.

Above the LCL, the parcel is checked for buoyancy using the condition

$$\theta_U^e > \theta_E^s, \quad (24)$$

where θ_E^s is the saturated equivalent potential temperature of the environment (the environmental θ_E^s is the grid element θ_G^s). This check begins at the first level above the LCL. The cloud top is given by the condition

$$\int_{\text{LCL}}^{\text{CT}} [T_U^s - T_E]\rho dz = 0, \quad (25)$$

where T_U^s is the temperature of a saturated updraft parcel and T_E the environmental temperature. This formulation permits overshooting tops.

Since the entrainment rate (22) is a function of the cloud depth, Eq. (25) must be solved iteratively. Furthermore, thermodynamic characteristics of the parcel are only known in terms of saturated equivalent potential temperature, and, therefore, updraft temperatures (T_U^s) and saturation mixing ratios (r_U^s) must be extracted iteratively using the Clausius-Clapeyron equation and the definition of θ^e.

Once the temperatures are extracted from θ_U^e, the distribution of vertical motion in the updraft is obtained from the "parcel" form of the vertical motion equation (see Hess, 1959). It is assumed that

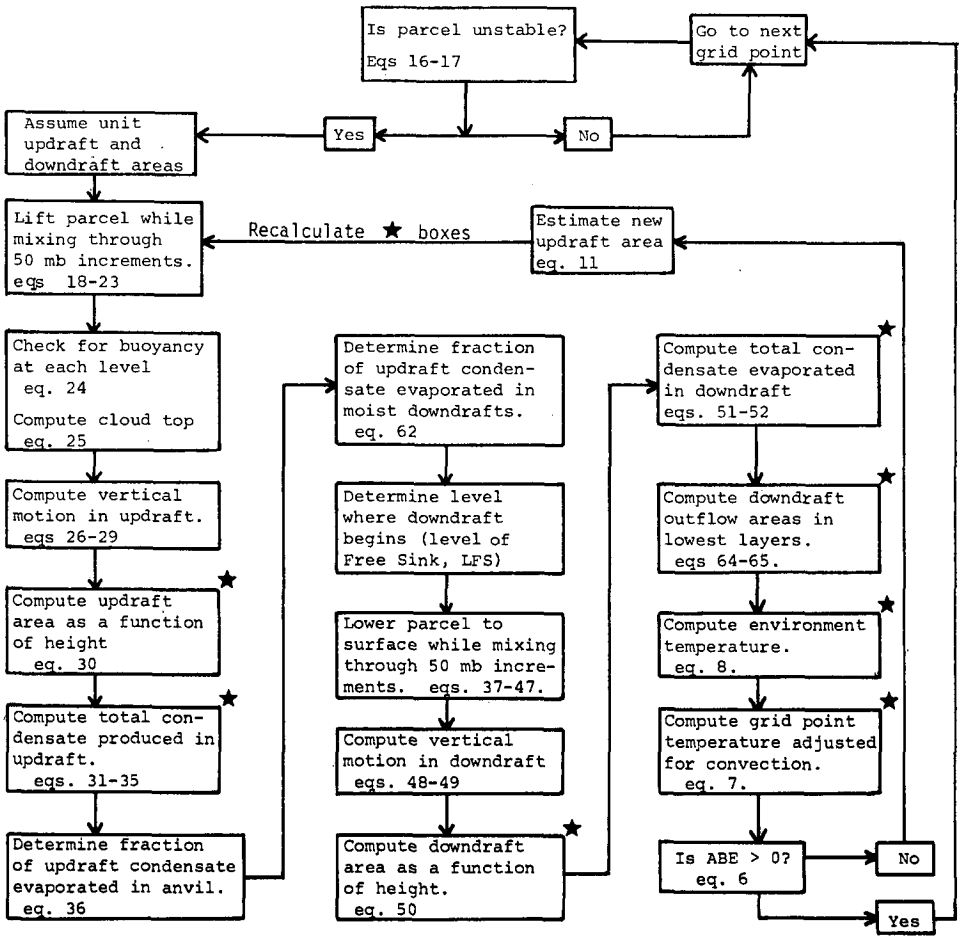

FIG. 3. Flow diagram of the cloud model and its interaction with the convective parameterization.

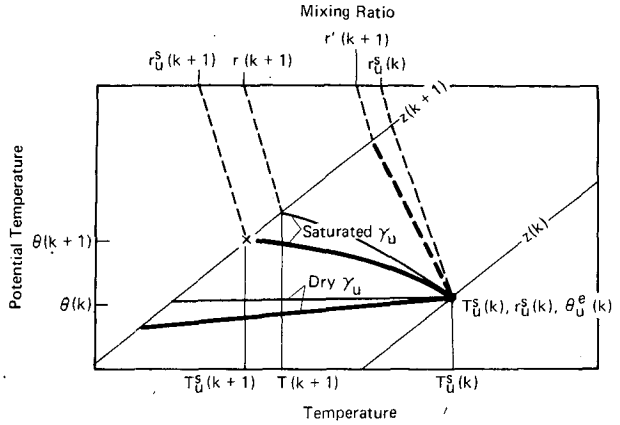

FIG. 4. Thermodynamic diagram of parcel ascent. Thin lines indicate ascent without entrainment; heavy lines include entrainment. Dashed lines are mixing ratio lines and solid lines indicate parcel temperature following saturated or dry ascent.

the environment is in hydrostatic balance and pressure perturbations due to the cloud are ignored. Therefore, vertical motion may be calculated from

$$w_U^2(k+1) = w_U^2(k) + 2g \int_{z(k)}^{z(k+1)} \frac{\tilde{T}_U(k) - \tilde{T}_E(k)}{\tilde{T}_E(k)}\, dz, \quad (26)$$

where

$$\tilde{T}_U(k) = \tfrac{1}{2}[T^s_U(k+1) + T^s_U(k)], \quad (27)$$

$$\tilde{T}_E(k) = \tfrac{1}{2}[T_E(k+1) + T_E(k)], \quad (28)$$

and w_U(LCL) is defined by

$$w_U^2(\mathrm{LCL}) = w_0^2 + 2g \int_{z_0}^{\mathrm{LCL}} \frac{T_U - T_E}{T_E}\, dz. \quad (29)$$

The level z_0 is the height of the bottom of the 100 mb layer which was found to be unstable; $w_0 = 1$ m s^{-1} and T_U is linearly interpolated between $T(z_0)$ and T_U(LCL) + ΔT.

Once the updraft vertical motion is obtained from (26) and (29), the updraft area can be determined from

$$A_U(k) = \frac{M_U(k)}{\rho_U(k) w_U(k)}, \quad (30)$$

where $\rho_U(k)$ is obtained from the equation of state assuming the pressure is the same in updraft and environment.

b. Rate of condensate production in the updraft

After the vertical distribution of θ^e_U and T^s_U for the entraining parcel ascent have been determined, the rate of condensate production in each cloud layer, $z(k+1) - z(k)$, is calculated. Fig. 4 is helpful in understanding the computational procedure described below.

Assuming that the updraft parcel remains saturated, the decrease in saturation mixing ratio over a layer is given by

$$\delta r^s_U(k) = r^s_U(k) - r^s_U(k+1), \quad (31)$$

where $r^s_U(k)$ is the updraft saturation mixing ratio at level k. Not all of this decrease is realized as condensate since the entrainment of drier air produces part of the decrease. For example, a parcel starting at level k with mixing ratio $r^s_U(k)$ arrives at level $k+1$ with the same mixing ratio if there is no condensation or entrainment (see Fig. 2). If entrainment occurs, but no condensation, then the parcel arrives with mixing ratio $r'(k+1)$ where

$$r'(k+1) = [r^s_U(k) M_U(k) + \Delta M_U(k) \tilde{r}_E] \times [M_U(k) + \Delta M_U(k)]^{-1}. \quad (32)$$

Since r^s_U is the mixing ratio of the parcel when it arrives at level $k+1$ and both condensation and entrainment have been included, the decrease in mixing ratio due to condensation is

$$\Delta r^s_U(k) = r'(k+1) - r^s_U(k+1). \quad (33)$$

Therefore, the rate of condensate production in the layer is

$$\Delta R_U(k) = \tilde{w}_U(k) \tilde{\rho}_U(k) \tilde{A}_U(k) \Delta r^s_U(k), \quad (34)$$

and for the entire updraft is

$$R_U = \sum_{k=\mathrm{LCL}}^{k=\mathrm{CT}} \Delta R_U(k). \quad (35)$$

c. Condensate lost in anvil

The anvil evaporation rate (A_e) is defined as minus the condensate production rate from the level of equilibrium temperature, ETL (updraft parcel temperature equals the environmental temperature) up to cloud top, or

$$A_e = \sum_{k=\mathrm{ETL}}^{k=\mathrm{CT}} \Delta R_U(k). \quad (36)$$

Total moisture evaporated from the anvil is given by A_e times the time of convection τ_c. This total amount is evaporated into the environment in increments corresponding to model time steps (30 s). For each time step, air outside the cloud anvil in the highest model layer occupied by convective clouds is saturated first. If the condensate increment is not totally evaporated in the highest layer, then successively lower layers are saturated.

d. Moist downdrafts

Normally there are two processes which initiate and maintain moist downdrafts; negative buoyancy from evaporational cooling and precipitation drag. In the formulation described below, only the nega-

tive buoyancy is included. Although precipitation drag is undoubtedly very important in some instances, it is assumed that it plays a secondary role in the type of midlatitude organized convection being considered here. Thus, the mid-level intrusion of relatively cool, dry environmental air into moist updraft air, and the subsequent evaporation of cloud droplets and rain falling from the updraft, are the only mechanisms included in the downdraft formulation.

The depth of the downdraft is specified by the level of free sink (LFS) and the surface. The level of free sink is where the temperature of a saturated mixture of equal amounts of updraft and environmental air becomes less than the environmental temperature. It is assumed that sinking motion begins with a downward velocity of 1 m s^{-1} at the LFS. The equivalent potential temperature is found there by mixing parcel and environment in equal amounts according to the technique developed by Foster (1958). Below the LFS, the downdraft parcel is lowered and mixed through ~50 mb increments down to the surface. The thermodynamic structure of the downdraft is determined in much the same manner as the updraft, except that a constant relative humidity for each layer is specified instead of always requiring saturated conditions. This approach crudely takes into account the facts that all downdraft air is not saturated nor does initially saturated air necessarily remain so during the entire downward path. In the initial model simulation (Fritsch and Chappell, 1980), the downdraft is assumed saturated above cloud base, while below it is assumed to be 80% of saturation.

The downdraft mixing ratio may change from both entrainment and evaporation. Once the relative humidity is specified for a layer and the change in mixing ratio due to entrainment is calculated, then the amount of evaporation necessary to produce the specified relative humidity can be determined. For example, using Fig. 5 as an aid, we consider a parcel originating at level k with a mixing ratio $r_D(k)$. The parcel will arrive at level $k-1$ with the same mixing ratio $[r_D(k)]$ if there is no entrainment or evaporation. If no evaporation occurs, but entrainment is included, the parcel will arrive at level $k-1$ with a different mixing ratio, $r'(k-1)$, where

$$r'(k-1) = \frac{r_D(k)M_D(k) + \Delta M_D(k)\bar{r}(k-1)}{M_D(k) + \Delta M_D(k)}, \quad (37)$$

$$\Delta M_D(k) = M_D(k-1) - M_D(k), \quad (38)$$

$$M_D(k) = [1 + K_D(k)]M_D(\text{LFS}), \quad (39)$$

$$k_D(k) = \sum_{q=k+1}^{q=\text{LFS}} \Delta K_D(q), \quad (40)$$

$$\Delta K_D(k) = B_D[z(k) - z(k-1)] \times [z(\text{LFS}) - z(\text{SFC})]^{-1}, \quad (41)$$

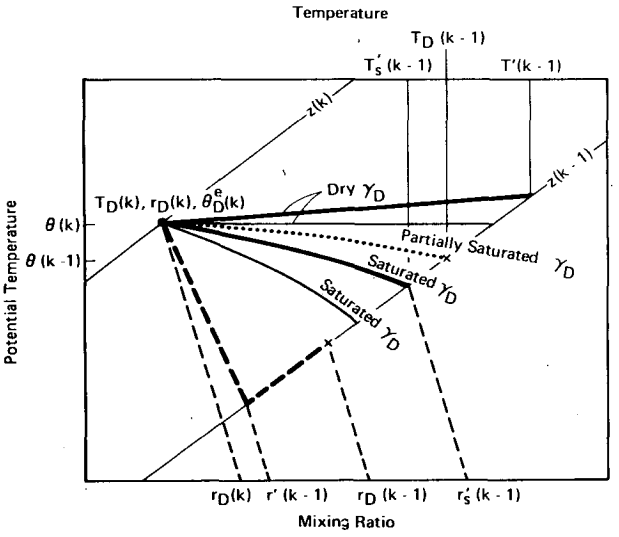

FIG. 5. Thermodynamic diagram of parcel descent. Thin lines indicate descent without entrainment; heavy lines include entrainment. Dashed lines are mixing ratio lines; solid lines indicate temperature of parcel following saturated or dry descent; dotted lines indicate partially saturated descent.

$$B_D = \frac{z(\text{LFS}) - z(\text{SFC})}{5.5 \times 10^5 \text{ cm}}. \quad (42)$$

The constant in (42) was selected to produce an entrainment rate which will double the downdraft mass if the parcel originates at ~500 mb. For this same entrainment rate, the equivalent potential temperature of the downdraft is obtained from

$$\theta_D^e(k-1) = [\theta_D^e(k)M_D(k) + \Delta M_D(k)\bar{\theta}_E^e(k-1)] \times [M_D(k) + \Delta M_D(k)]^{-1}. \quad (43)$$

The entraining parcel mixing ratio, $r'(k-1)$, is the minimum ratio that can occur as the parcel arrives (with no evaporation) at level $z(k-1)$. The maximum mixing ratio $r_s'(k-1)$ and the coldest possible temperature $T_s'(k-1)$ that an entraining parcel can have, occur if the parcel evaporates enough condensate to remain saturated. Assuming saturation is maintained in the layer k to $k-1$, $r_s'(k-1)$ and $T_s'(k-1)$ can be iteratively extracted from $\theta_D^e(k-1)$ using the Clausius-Clapeyron equation. If the relative humidity (RH) is specified, then the new mixing ratio for descent with partial saturation is simply

$$r_D(k-1) = \text{RH}\, r_s'(k-1). \quad (44)$$

The amount of evaporation Δr_D is the difference between $r_D(k-1)$ and the parcel mixing ratio with entrainment but no evaporation, i.e.,

$$\Delta r_D(k) = r_D(k-1) - r'(k-1). \quad (45)$$

Finally, the temperature of the downdraft parcel,

$T_D(k-1)$, is given by

$$T_D(k-1) = T_s'(k-1) + \delta T, \tag{46}$$

where

$$\delta T = \frac{L}{c_p}[r_s'(k-1) - r_D(k-1)]. \tag{47}$$

Again using the parcel method as described for the updraft, vertical motion is calculated from

$$w_D^2(k-1) = w_D^2(k) + 2g\int_{z(k)}^{z(k-1)} \frac{\tilde{T}_D(k) - \tilde{T}_E(k-1)}{\tilde{T}_E(k-1)}\,dz, \tag{48}$$

where

$$\tilde{T}_D(k) = \tfrac{1}{2}[T_D(k-1) + T_D(k)], \tag{49}$$

and $\tilde{T}_E(k-1)$ is defined by (28). At the surface, w_D is set to zero.

Knowing the downdraft temperature from (46) and the mass flux from (39), the downdraft area can be obtained from

$$A_D(k) = \frac{M_D(k)}{\rho_D(k) w_D(k)}, \tag{50}$$

where $\rho_D(k)$ is determined from the equation of state assuming the pressure is the same in downdraft and environment.

e. Rate of condensate loss in the downdraft

The rate of condensate loss for each layer is given by

$$\Delta R_D(k) = \tilde{w}_D(k)\,\tilde{\rho}_D(k)\,\tilde{A}_D(k)\,\Delta r_D(k), \tag{51}$$

where $\Delta r_D(k)$ is given by (45). The condensate loss for the entire downdraft is then

$$R_D = \sum_{k=2}^{k=\mathrm{LFS}} \Delta R_D(k). \tag{52}$$

f. Freezing and melting

Warming and cooling due to freezing and melting of condensate in the updraft and downdraft are also included in the model. In the updraft, the freezing level (FL) is arbitrarily specified ($T_U = -25$°C) and all (or a fraction) of the condensate produced below this level is instantaneously frozen as it passes upward through the FL. At this point the latent heat of freezing is released and a new pseudoadiabat (θ^e) is determined for the parcel. The amount of condensate (C_f) which is frozen is given by

$$C_f = \sum_{k=\mathrm{LCL}}^{k=\mathrm{FL}-1} \Delta r_U^s(k)\left[1 + \frac{L}{c_p}\frac{\partial r^s}{\partial T}\right]^{-1}, \tag{53}$$

which produces a parcel temperature change ΔT where,

$$\Delta T = [L_{\mathrm{ice}} - L_{\mathrm{water}}]C_f/c_p, \tag{54}$$

$$L_{\mathrm{ice}} = 677.0 - 0.062(T - 273)\ [\mathrm{cal\ g^{-1}}], \tag{55}$$

$$L_{\mathrm{water}} = 597.3 - 0.566(T - 273)\ [\mathrm{cal\ g^{-1}}]. \tag{56}$$

The condensate which is melted in the downdraft is given by

$$C_m = \sum_{k=2}^{k=\mathrm{ML}} \Delta r_D(k)\left[1 + \frac{L}{c_p}\frac{\partial r^s}{\partial T}\right]^{-1}, \tag{57}$$

where ML is the melting level defined as $z(T = 0$°C).

g. Relationship of downdraft mass flux to updraft

An expression can now be derived for the number of units of downdraft air that results from each unit of updraft air. From Fig. 2, the precipitation efficiency E is approximated by

$$E = 1.591 - 0.639\frac{\Delta V}{\Delta z} + 0.0953\left(\frac{\Delta V}{\Delta z}\right)^2 - 0.00496\left(\frac{\Delta V}{\Delta z}\right)^3, \tag{58}$$

and

$$E = 0.9 \quad \text{for} \quad \frac{\Delta V}{\Delta z} < 1.35,$$

where $\Delta V/\Delta z$ is the vertical shear of the horizontal wind evaluated over the cloud depth and has the units 10^{-3} s^{-1}. The rate of supply (S) of moisture to the updraft is defined as the sum of the vertical flux of vapor and liquid at ~150 mb above the LCL:

$$S = \rho_U w_U r_U A_U\big|_{z(\mathrm{LCL}+3)} + \sum_{k=\mathrm{LCL}}^{K=\mathrm{LCL}+2} \Delta R_U(k). \tag{59}$$

The convective precipitation rate (P_r) is then

$$P_r = E\,S \tag{60}$$

and the rate of condensate evaporation (C_e) is

$$C_e = R_U - P_r. \tag{61}$$

Of this amount, part is lost to the downdraft and the remainder goes out the anvil. The anvil evaporation rate (A_e) was defined in (36) so that the rate of condensate evaporated in the downdraft (D_e) can be written

$$D_e = C_e - A_e, \tag{62}$$

and the number of units of downdraft (N_D) per unit of updraft is

$$N_D = D_e/R_D = (R_U - E\,S - A_e)/R_D. \tag{63}$$

h. Downdraft outflow

As the moist downdraft within a numerical model grid column approaches the surface, it begins to diverge and spread out into a relatively shallow layer, usually no deeper than ~1 km. The cloud model crudely simulates this effect in individual

grid elements by calculating the total mass brought down in the downdraft and successively replacing environmental air in grid element layers (starting with the lowest layer) until the downdraft mass is accounted for.

The total downdraft mass (μ) is defined by

$$\mu = -\tau_c[\rho_D w_D A_D]_{k=2}. \tag{64}$$

The mass needed to fill (replace environmental air by downdraft air) layer k of a grid element is

$$\nu(k) = \tilde{\rho}_D(k + 1)\,\Delta z(k)\,A, \tag{65}$$

so that the number of layers and respective downdraft areas are easily determined. Normally, the lowest two layers are sufficient to contain the downdraft outflow.

i. Momentum transport

Environmental momentum is mixed into cloud parcels in the same manner that the equivalent potential temperature of cloud and environment are mixed:

$$\left.\begin{aligned} u_U(k+1) &= [u_U(k)M_U(k) + \Delta M_U(k)\tilde{u}_E(k)] \\ &\quad \times [M_U(k) + \Delta M_U(k)]^{-1} \\ v_U(k+1) &= [v_U(k)M_U(k) + \Delta M_U(k)\tilde{v}_E(k)] \\ &\quad \times [M_U(k) + \Delta M_U(k)]^{-1} \end{aligned}\right\}, \tag{66}$$

$$\left.\begin{aligned} u_D(k-1) &= [u_D(k)M_D(k) + \Delta M_D(k)\tilde{u}_E(k-1)] \\ &\quad \times [M_D(k) + \Delta M_D(k)]^{-1} \\ v_D(k-1) &= [v_D(k)M_D(k) + \Delta M_D(k)\tilde{v}_E(k-1)] \\ &\quad \times [M_D(k) + \Delta M_D(k)]^{-1} \end{aligned}\right\}. \tag{67}$$

The initial momentum of the updraft parcel is obtained by mixing the momentum in the 100 mb layer which was found to be thermodynamically unstable. The initial downdraft momentum is derived from an equal mixture of updraft air and environmental air in the 50 mb layer which contains the level of free sink.

4. Summary and conclusions

A parameterization formulation for incorporating the effects of midlatitude deep convection into mesoscale numerical models is presented. The formulation is based on the hypothesis that the buoyant energy available to a parcel, in combination with a prescribed period of time for the convection to remove that energy, can be used to regulate the convection in a *mesoscale* numerical model grid element. The following assumptions and constraints summarize the main features of the parameterization:

(i) Moist convection only occurs when air is forced to its level of free convection by low-level convergence, air mass overrunning, or when low-level heating and mixing remove any stable layers suppressing moist convection (i.e., when potential buoyant energy becomes available).

(ii) Mass transports by moist convection are closely approximated by a model cloud ensemble which treats *deep* convection as the dominant cloud form.

(iii) Precipitation efficiency of the convective clouds is related to the vertical wind shear across the cloud depth.

(iv) The grid-scale stabilization rate (destruction of ABE) by moist convective processes is equivalent to minus the model generated ABE divided by the estimated time for the convective cells to move across the grid element. This time period τ_c is obtained by dividing the grid length by the mean environmental wind speed over the cloud depth; τ_c has a lower limit defined by the average lifetime of individual cells (30 min), and an upper limit (1 h) to allow large-scale changes to alter the characteristics of the convective clouds. If the period of time necessary to consume all of the ABE is greater than 1 h, the computed rate of stabilization is still applied for 1 h, even though all the ABE will not be consumed. After 1 h, the atmosphere is again checked for instability and convection may be initiated once again (at different adjustment rates, however).

(v) The vertical distribution of the convective heating and cooling of environmental air is the resultant structure that occurs when 1) the cloud model processes sufficient mass to produce the net stabilization by moist convection as specified in (iv) above; and 2) the environmental vertical motion field adjusts to the mass requirements of the convective cloud model and the larger scale vertical transports.

(vi) The changes in temperature and mixing ratio at a model grid point are the sum of the effects of compensating subsidence in the environment plus the effect of area-weighting the cloud updraft, downdraft and environment.

(vii) Momentum is vertically exchanged through bulk mixing processes in the cloud updrafts and downdrafts and by compensating environmental vertical motions.

Whereas most other parameterization techniques try to maintain some type of balance between the large-scale rate of destabilization and the rate of convection, the formulation presented above recognizes that *convection responds not only to the rate at which the large scale is generating buoyant energy, but also to the buoyant energy generated and stored prior to the onset of deep convection.*

Initial testing of the parameterization formulation has been carried out in a mesoscale primitive equation model using analytical initial conditions. Re-

sults of a model simulation are presented in Part II of this paper (Fritsch and Chappell, 1980). In general, the results demonstrate that the parameterization is capable of generating convectively driven mesoscale pressure systems. Further testing of the parameterization is planned using a different formulation for the precipitation efficiency of the convective clouds. Rather than using only the vertical shear of the horizontal wind to specify precipitation efficiency, effects of cloud base height (from Fujita, 1959) will be incorporated. Also, testing with real data cases to check timing, amplitude and phase speed of the convectively generated mesoscale disturbances will be undertaken.

Acknowledgments. The authors gratefully acknowledge the support and contributions from Lewis O. Grant, Wayne H. Schubert and Alan K. Betts. Frequent enlightening discussions with Everett C. Nickerson, L. Ray Hoxit and Robert A. Maddox are also greatly appreciated. Particular thanks are extended to Richard A. Anthes, Roger A. Pielke, William R. Cotton, Stephen M. Wandzura and especially John M. Brown for the rigorous reviews of the manuscript and numerous helpful suggestions. Ms. Irene Bork skillfully prepared the manuscript.

APPENDIX

List of Symbols

A	area of model grid element
ABE	available buoyant energy
A_e	anvil evaporation rate
B_D	bulk mixing coefficient for convective downdrafts
B_U	bulk mixing coefficient for convective updrafts
c_p	specific heat at constant pressure
C_e	condensate evaporation rate
C_f	amount of condensate which is frozen in the updraft
C_m	amount of condensate which is melted in the downdraft
CT	convective cloud-top height
C^*	local condensation or evaporation rate
D_e	downdraft evaporation rate
E	precipitation efficiency of convective clouds
ETL	equilibrium temperature level for convective updraft
FL	freezing level in convective updrafts
g	gravity
K_D	downdraft entrainment coefficient
K_U	updraft entrainment coefficient
L	latent heat of condensation
L_{ice}	latent heat of condensation plus fusion
L_{water}	latent heat of condensation
LCL	lifting condensation level
LFC	level of free convection
LFS	level of free sink
M	vertical mass flux
ML	melting level in convective downdrafts
N	number of updraft-downdraft "cloud" units
N_D	number of units of downdraft air per unit of updraft air
p	pressure
P_r	convective precipitation rate
PBE	potential buoyant energy
r	mixing ratio
R	dry air gas constant
RH	relative humidity
R_D	rate of condensate loss due to evaporation in convective downdrafts
R_U	rate of condensate production in convective updrafts
S	rate of supply of moisture to cloud updrafts
SFC	surface, lowest level in model
T	temperature
t	time
u	x component of horizontal wind
v	y component of horizontal wind
V	scaler magnitude of horizontal wind
$\mathbf{V}$	vector wind
w	vertical component of wind
β	$T_U - T$
γ	environmental lapse rate
Γ	dry adiabatic lapse rate
μ	total downdraft mass
ρ	density
τ_c	period of time convection is active in a grid element
θ	potential temperature
θ^e	equivalent potential temperature
ν	mass needed to fill a grid element volume with downdraft air
ω	vertical motion in pressure coordinates

Mathematical operators and symbols

A	area of integration; area of a model grid element
dz	incremental height
δ	incremental change
Δ	finite-difference approximation to the partial derivative

Coordinates

z	Cartesian coordinate, increases with height

Subscripts

D	variables of the convective downdraft
E	variables of the convective environment
G	grid element value of a variable
k	coordinate of a grid point in the z direction (numbered from the surface)
0	indicates lowest level where updraft originates

s denotes saturation with respect to water vapor
U variables of the convective updraft

Superscripts

m iteration number in determining the amount of convective mass transport
s denotes saturation with respect to water vapor

Symbol variations

caret adjusted for the effects of convection
tilde vertical average over a model layer, k, $k+1$

REFERENCES

Anthes, R. A., 1977: A cumulus parameterization scheme utilizing a one-dimensional cloud model. *Mon. Wea. Rev.*, **105**, 270–286.

Arakawa, A., and W. H. Schubert, 1974: Interaction of a cumulus cloud ensemble with the large-scale environment. Part I. *J. Atmos. Sci.*, **31**, 674–701.

Auer, A. H., and J. D. Marwitz, 1968: Estimates of air and moisture flux into hailstorms on the high plains. *J. Appl. Meteor.*, **7**, 196–198.

Byers, H. E., 1951: Thunderstorms. *Compendium of Meteorology*, Amer. Meteor. Soc., 681–693.

Caracena, F., R. Maddox, L. R. Hoxit and C. F. Chappell, 1979: Mesoanalysis of the Big Thompson storm. *Mon. Wea. Rev.*, **107**, 1–17.

Ceselski, B. F., 1974: Cumulus convection in weak and strong tropical disturbances. *J. Atmos. Sci.*, **31**, 1241–1255.

Chang, C. P., and T. M. Piwowar, 1974: Effect of a CISK parameterization on tropical wave growth. *J. Atmos. Sci.*, **31**, 1256–1261.

Charney, J. G., and A. Eliassen, 1964: On the growth of the hurricane depression. *J. Atmos. Sci.*, **21**, 68–75.

Chen, C., and H. D. Orville, 1980: Effects of mesoscale convergence on cloud convection. *J. Appl. Meteor.*, **19** (in press).

Chisholm, A. J., 1970: Alberta hailstorms: A radar study and model. Ph.D. thesis, McGill University, 237 pp.

Fankhauser, J. C., 1971: Thunderstorm-environment interactions determined from aircraft and radar observations. *Mon. Wea. Rev.*, **99**, 171–192.

Foote, G. B., and J. C. Fankhauser, 1973: Airflow and moisture budget beneath a northeast Colorado hailstorm. *J. Appl. Meteor.*, **12**, 1330–1353.

Foster, D. S., 1958: Thunderstorm gusts compared with computed downdraft speeds. *Mon. Wea. Rev.*, **86**, 91–94.

Fraedrich, K., 1974: Dynamic and thermodynamic apsects of the parameterization of cumulus convection. Part II. *J. Atmos. Sci.*, **31**, 1838–1849.

Fritsch, J. M., and C. F. Chappell, 1980: Numerical prediction of convectively driven mesoscale pressure systems. Part II: Mesoscale model. *J. Atmos. Sci.*, **37**, 1734–1762.

——, —— and L. K. Hoxit, 1976: The use of large scale budgets for convective parameterization. *Mon. Wea. Rev.*, **104**, 1408–1418.

Fujita, T., 1959: Precipitation and cold air production in mesoscale thunderstorm systems. *J. Meteor.*, **16**, 454–466.

Gadd, A. J., and E. M. Newson, 1969: Surface exchanges of sensible and latent heat in a 10 level model atmosphere. *Quart. J. Roy. Meteor. Soc.*, **96**, 297–308.

Hartsell, C., 1970: Case study of a traveling hailstorm. Rep. No. 70-1, Inst. Atmos. Sci., South Dakota School of Mines and Technology, 72 pp.

Hess, S. L., 1959: *Introduction to Theoretical Meteorology*. Holt, Rinehart and Winston, 362 pp.

Johnson, R. H., 1976: The role of convective-scale precipitation downdrafts in cumulus and synoptic-scale interactions. *J. Atmos. Sci.*, **33**, 1890–1910.

Kreitzberg, C. W., and D. J. Perkey, 1976: Release of potential instability: Part I. A sequential plume model within a hydrostatic primitive equation model. *J. Atmos. Sci.*, **33**, 456–475.

Kuo, H. L., 1965: On the formation and intensification of tropical cyclones through latent heat release by cumulus convection. *J. Atmos. Sci.*, **22**, 40–63.

——, 1974: Further studies of the parameterization of the influence of cumulus convection on large-scale flow. *J. Atmos. Sci.*, **31**, 1232–1240.

Manabe, S., J. Smagorinsky and R. R. Strickler, 1965: Simulated climatology of a general circulation model with a hydrologic cycle. *Mon. Wea. Rev.*, **93**, 769–798.

Marwitz, J. O., 1972: Precipitation efficiency of thunderstorms on the High Plains. *J. Rech. Atmos.*, **6**, 367–370.

Mintz, Y., 1965: Very long global integration of the primitive equations of atmospheric motion. WMO Tech. Note No. 66, 141–167.

Newton, C. W., 1966: Circulations in large sheared cumulonimbus. *Tellus*, **18**, 699–712.

Ogura, Y., and H. R. Cho, 1973: Diagnostic determination of cumulus cloud populations from observed large-scale variables. *J. Atmos. Sci.*, **30**, 1276–1286.

Oliger, J. E., R. E. Wellick, A. Kasahara and W. M. Washington, 1970: Description of NCAR global circulation model. NCAR TN/STR-56, 94 pp.

Ooyama, K., 1963: A dynamic model for the study of tropical cyclone development. Dept. Meteor. Oceanogr., New York University. [Available upon request from K. Ooyama, National Center for Atmospheric Research, Boulder, CO 80302.]

——, 1969: Numerical simulation of the life cycle of tropical cyclones. *J. Atmos. Sci.*, **26**, 3–40.

——, 1971: A theory on parameterization of cumulus convection. *J. Meteor. Soc., Japan*, **39**(Special issue), 744–756.

Rosenthal, S. L., 1970: Experiments with a numerical model of tropical cyclone development: Some effects of radial resolution. *Mon. Wea. Rev.*, **98**, 106–121.

Rossby, C. G., 1932: Thermodynamics applied to air mass analysis. *MIT Meteor. Pap.*, **1**, No. 3, 48 pp.

Smagorinsky, J., 1956: On the inclusion of moist adiabatic processes in numerical prediction models. *Ber. Dtsch. Wetterdienstes*, **5**, 82–90.

Yamasaki, M., 1968: A tropical cyclone model with parameterized vertical partition of released latent heat. *J. Meteor. Soc. Japan*, **46**, 202–214.